Control topology for high efficiency small scale wind energy conversion systems

Stefan Daraban, Dorin Petreus, Cristian Orian
Technical University of Cluj Napoca, Cluj-Napoca, Romania
stefan.daraban@ael.utcluj.ro

Abstract-This paper will present the importance of control topology for power systems used in wind energy conversion systems (WECS). The efficiency and the method of sizing the components of the system are different from one control method to the other. Also a control method is proposed and analysed by using a power factor correction (PFC) controller in a novel configuration suitable for modular design. By using modular design, the same converter can be used in multiple applications. A wind model is used in order to better simulate the behaviour of the system and test the MPPT algorithms. The experimental results validate the theoretical and simulated ones.

I. INTRODUCTION

In wind energy conversion systems (WECS) the wind power is transformed into a form of energy that can be used by humans: electrical power (wind turbines), mechanical power (windmills), etc. Because of the new policies on the environment regarding the energy production, WECS gained a lot of popularity. Offshore wind farm are placed near the oceans and seas where the winds are higher and steadier [1].

The easiest way to implement a low cost and low power (2kW) WECS system is to use a passive rectifier after the generator and then a step up converter followed by the inverter [2].

In [3] the authors propose to use the phase inductance of the generator as the inductor of the Boost converter. The system is able to harvest up to 1.2 KW and eliminates the input filter capacitor and the Boost inductor, thus reducing the cost of the system. The disadvantages are the low gain and reduced efficiency compared to the conventional Boost converter.

Single stage converters can also be used after the rectifier. A topology that is used with solar panels is the flying inductor topology [4]. This topology has good dynamics but has a low efficiency.

A low cost WECS composed from a rectifier implemented with diodes and a single phase inverter is proposed in [5]. The advantages are the reduced costs and the simple control of the system. The disadvantages are: a very high total harmonic distortion (THD) factor of the output current (that makes it impossible to be sold on the market) and only a part of the total available mechanical power of the turbine can be extracted. The low output voltage limit of the rectifier is limited to a value that makes the inverter stage still operable.

In order to prevent the under voltage protection of the inverter, a Boost stage is introduced. The system with two power stages achieves good performances (good energy harvesting capability and small THD) with simple control (no need for information of torque and speed) [6].

For higher power levels (10kW), in [7] is implemented a back to back converter. This converter has the highest energy harvesting capability but it has a very complex control structure. Some other topologies that are used in high power WECS are: Vienna rectifier [8], matrix converter [9] and multilevel converters [10]. Another concept used in applications that need rectifiers, is to treat each phase independently from each other [11].

In order for the system to be able to extract the maximum power from the wind turbine, the power system has to have a maximum power point tracking (MPPT) controller. The control topology has a great influence on the dynamics and on the cost of the system. The control method depends on the MPPT algorithm that is implemented on the system. A classification of the MPPT algorithms for WECS is presented in [12].

The power signal feedback control (PSF) algorithm needs to know in advance the locus of the P-ω characteristic which can be obtained by simulations or experimental measurements. Accurate determination of the power locus is affected by atmospheric conditions.

The tip speed ratio control method uses a speed reference, obtained from wind speed measurements and a known optimum tip speed ratio. Because a speed loop is needed, the system needs a speed transducer, thus increasing the overall costs. The measurement of the wind speed is not very precise (due to the influence of the turbine blades) and an anemometer is needed, which will also increase the costs. An advantage is the fast dynamics of the system.

The MPPT algorithm that offers the greatest flexibility in the implementation and has the lowest manufacturing costs is the Hill Climb Search (HCS). This algorithm is very much alike with the Perturb and Observe (P&O) that is used in photovoltaic applications. In order to harvest more energy a P&O with variable step was implemented in [13]. For a better testing of the MPPT algorithm in WECS, wind models have been created in [14].

The paper has six main sections. Firstly the power and the control topologies are analysed, followed by the next section that examines the proposed control topology. Two MPPT algorithms (Perturb & Observe and Power Signal Feedback) are presented next. Two important sections are the simulations and experimental results that prove the applicability of the chosen control topology.

978-1-4799-5183-3/14/$31.00 ©2014 IEEE

II. POWER AND CONTROL TOPOLOGIES

The system that will be used to test the importance of the control topology in a WECS is composed of a passive rectifier, a step up converter, a step down converter and an unfolding bridge. The overall system schematic is presented in Fig. 1. The generator is a synchronous machine with permanent magnets.

A transformerless topology is used to obtain a high efficiency system. For the first power stage a Boost converter is used to step up the voltage from the wind turbine because it is not high enough to directly connect the inverter. For better efficiency an interleaved Boost converter can be used [15]. The following converter topologies have been tested for the inverter: Buck, interleaved Buck and Coolcept [16].

The article proposes a fourth topology in which the inductors from the Coolcept topology are coupled. This topology is presented in Fig. 2. The advantages of coupling the inductors are: 1) from the point of view of the small signal model the two separate converters will works as one converter and have the dynamic response of a Buck converter with an inductor four time smaller; 2) the inputs (V_{C1}, V_{C2}) and outputs (V_{C3}, V_{C4}) voltages will balance in a shorter time; 3) the use of a lower inductance in order to obtain the same current ripple.

The Coolcept topology is property of Steca Elektronik GmbH and is used as grid tied inverter for photovoltaic applications. Because of its high efficiency, the Coolcept inverter will be used to implement a wind energy conversion system.

The roles of the second power stage are: to inject power into the grid and for power decoupling (eliminate the ripple at twice the grid frequency of the input voltage).

There are two symmetrical Buck converters which are placed one on top of the other. By dividing the input and output voltage in half for the two converters, semiconductors with lower voltage rating can be used, thus leading to higher performances. The C_1 and C_2 are electrolytic capacitors.

The duty cycle of the Coolcept topology varies with the output voltage:

$$d_{buck}(\omega t) = \frac{V_{out} \cdot |\sin(\omega t)|}{V_{bus}} \tag{1}$$

where V_{bus} is the DC bus voltage at the input of the inverter, V_{out} is the amplitude of the grid voltage and ω is the grid angular frequency.

A comparison is made between all the before mentioned step-down converters. The Buck converter is taken as reference. The normalised ripple current for all four topologies is represented in Fig. 3. The lowest ripple current is obtained by using the proposed coupling method for the Coolcept topology. The equations that describe the normalised ripple are:

$$\Delta i_{L\_Buck} = \frac{V_{in} \cdot d \cdot (1-d) \cdot T_{sw}}{L_{ind} \cdot \Delta i_{L\max}} \tag{2}$$

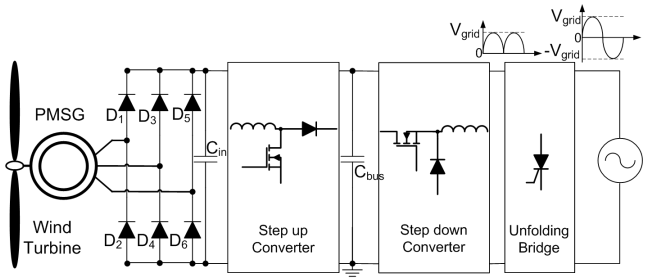

Fig. 1. Overall system schematic.

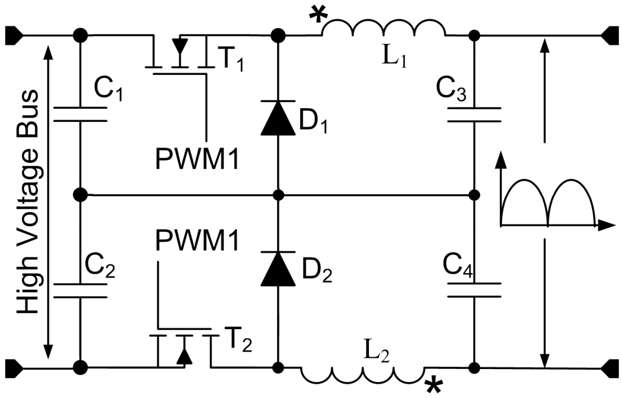

Fig. 2. Coolcept topology with coupled inductors.

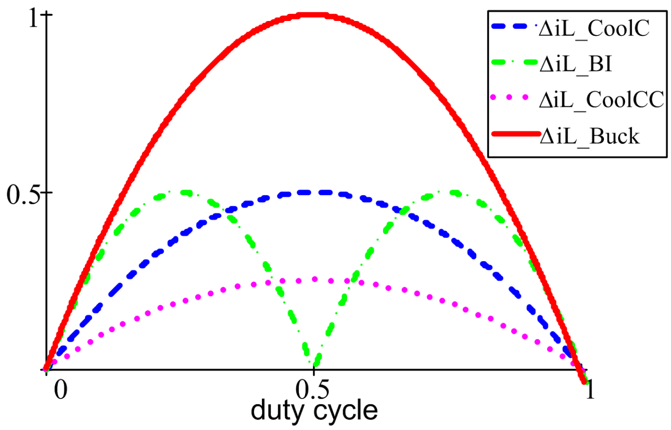

Fig. 3. Normalized inductor current ripple.

$$\Delta i_{L\_CoolC} = \frac{V_{in} \cdot d \cdot (1-d) \cdot T_{sw}}{2 \cdot L_{ind} \cdot \Delta i_{L\max}} \tag{3}$$

$$\Delta i_{L\_CoolCC} = \frac{V_{in} \cdot d \cdot (1-d) \cdot T_{sw}}{4 \cdot L_{ind} \cdot \Delta i_{L\max}} \tag{4}$$

$$\Delta i_{L\_BI} = \begin{cases} \Delta i_{L\_Buck} - \dfrac{V_{in} \cdot d^2 \cdot T_{sw}}{L_{ind} \cdot \Delta i_{L\max}}, d < 0.5 \\ \Delta i_{L\_Buck} - \dfrac{V_{in} \cdot (1-d)^2 \cdot T_{sw}}{L_{ind} \cdot \Delta i_{L\max}}, d > 0.5 \end{cases} \tag{5}$$

where Δi_{Lmax} is the maximum possible ripple, $\Delta i_{L\text{-}Buck}$ is the normalised ripple for the Buck converter, $\Delta i_{L\text{-}CoolC}$ is the normalised ripple for the Coolcept topology, $\Delta i_{L\text{-}CoolCC}$ is the normalised ripple for the proposed topology, $\Delta i_{L\text{-}BI}$ is the normalised ripple for the interleaved Buck converter, d is the duty cycle of the converter, V_{in} is the input voltage of the converter and T_{sw} is the switching period of the converter.

The interleaved Buck converter divides the power between its phases but it uses high voltage devices that do not offer the same performances as the lower rated devices from the Coolcept topology. The interleaved Buck would need more than two phases to have the same performances as the Coolcept topology but the size of the layout and the cost increase.

A total of three control topologies will be described next. The performances will be evaluated from the point of view of their dynamics, reliability and efficiency of MPPT algorithm.

There are three possible ways to control an energy conversion system with two power stages: 1) the DC bus is maintained by the step up converter; 2) the DC bus is maintained by the step down converter; 3) none of the converters regulate the DC bus.

The first control method features a high DC bus (400V) and the MPPT algorithm is computed on the inverter side. The schematic is illustrated in Fig. 4. The Boost converter implements an average current mode control to maintain its output voltage at 400V. The inverter implements a voltage loop on the input voltage. The reference is received from the MPPT algorithm that senses the input voltage and current. A synchronisation is made with the output voltage. The reference of the current loop is the output of the voltage loop (of the inverter) multiplied with the output of the PLL (|sin(ωt)|).

Because the inverter controls the input voltage and also the output current of the system and the Boost converter controls the input voltage of the inverter, inter-dependency between the two converters exists. The system has good dynamics but because of the inter-dependency between converters, the C_{bus} capacitor can not decouple the first power stage. The input voltage will have a ripple at twice the grid frequency.

The second control topology is presented in Fig. 5. The power stage is the same but now there is no inter-dependency between the two power stages. The Boost converter has three control loops: a power loop for the MPPT algorithm, a voltage loop on the input voltage and a current loop to protect the system from short circuit conditions. The inverter controls the DC bus and the output current. The current loop of the inverter is the same with the one used in the previous method.

The C_{bus} capacitor decouples the input power stage and there is no sinusoidal ripple at twice the grid frequency on the input voltage. The DC bus is calculated with:

$$C_{bus} = \frac{P_{in}}{2 \cdot \omega \cdot V_{in} \cdot \Delta V_{bus}} \tag{6}$$

where P_{in} is the input power and ΔV_{bus} is the accepted ripple on the DC bus.

The third control topology is presented in Fig. 6. There is a significant difference between this topology and the previous two control structures. It can be seen that even though the power stage is the same, this structure does not have a DC bus. The system will work either in Buck mode or in Boost mode and the other converter is bypassed. The C_{bus} capacitor will have a small value and the C_{in} capacitor will have a high value because this will be the decoupling capacitor.

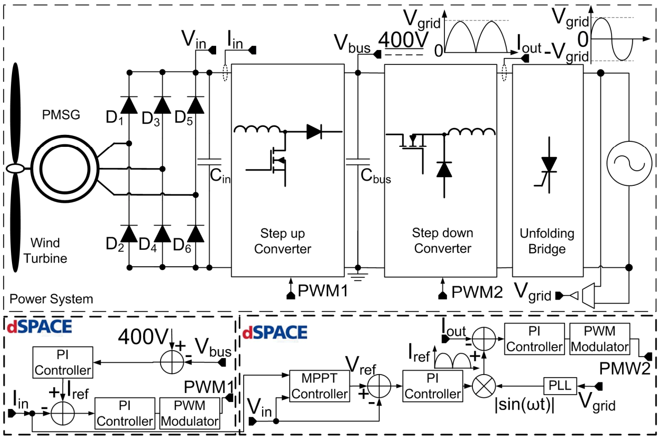

Fig. 4. MPPT control applied on the step down converter with a DC bus.

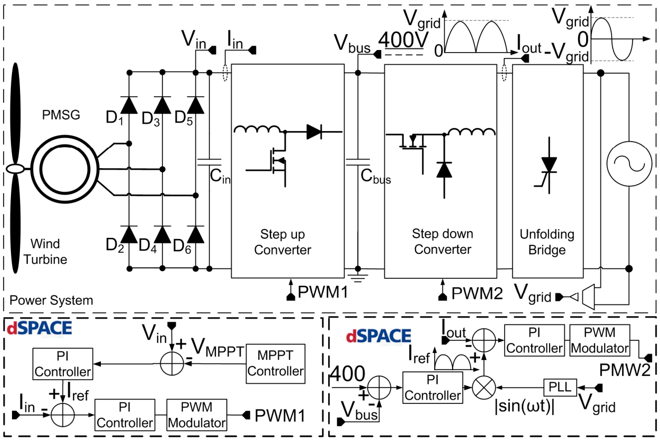

Fig. 5. MPPT control applied on the step up converter with a DC bus.

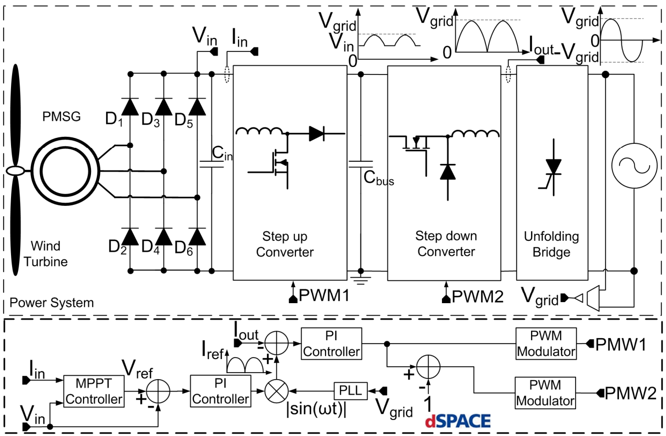

Fig. 6. MPPT control applied on the step up converter without a DC bus.

The efficiency of the system with the third control structure is higher because the energy passes through only one power stage at a time. The stability of the system and its dynamics are its disadvantages.

The best solution for a high efficiency WECS is the second control topology. It has good dynamics and there is no inter-dependency between the two systems. Even though the same power topology is used, the performances vary for each control structure. The design of the passive elements (inductors and capacitors) varies with the control topology. Each control structure has its advantages and disadvantages.

In the next section the proposed control topology will be presented and analysed.

III. Proposed Control Topology

The Coolcept inverter is an example of modular design. This converter can be used for multiple purposes: string inverter for PV panels (scans the entire characteristic of the photovoltaic panels for searching the global maximum power point in case of partial shading) or it can be used for a general purpose inverter for WECS or PV systems.

In order to use the Coolcept system for wind energy conversion, the inverter is configured to maintain its input voltage constant. The MPPT algorithm is implemented on the step-up converter.

The proposed control topology for modular design is build around the UC3854 power factor controller. The simplified schematic of the step-up converter with UC3854 is presented in Fig. 7.

The novelty of the proposed control structure is that both converters will control the DC bus at a certain moment in time. The Boost converter will control the DC bus first in order to assure a proper start up of the inverter.

For an easy explanation of the proposed topology, in Fig. 7 each control loop is represented in a different colour. The electronic components marked with red (A_1, R_{fi1}, C_{fi1}, R_{fi2} and C_{fi2}) form the current control loop. Depending on the operating state, the I_{REF} node is controlled by the voltage loop (blue) that regulates the Boost converter's output (A_2, R_{fv}, C_{fv}, R_5 and R_6) or by the MPPT controller marked with orange (MPPT algorithm and D_7) that set the I_{MPPT} current.

In Fig. 8 is presented the start-up sequence of the system and how the current reference node (I_{REF}) changes. For simplification, the inverter is modelled like a voltage source (because of its internal voltage loop that imposes the voltage on the DC bus).

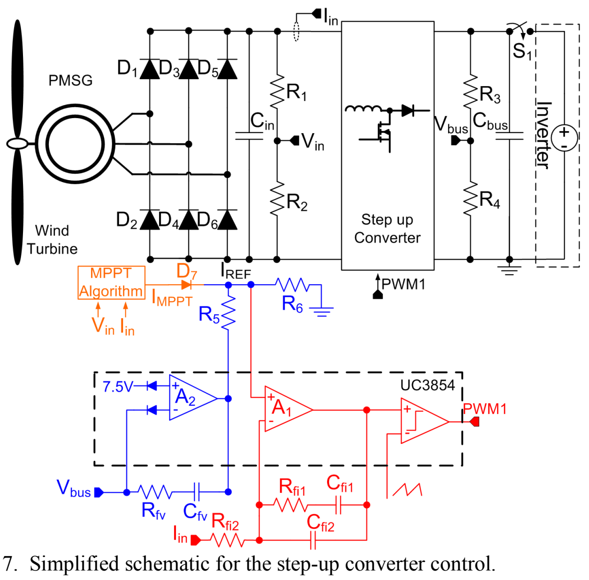

Fig. 7. Simplified schematic for the step-up converter control.

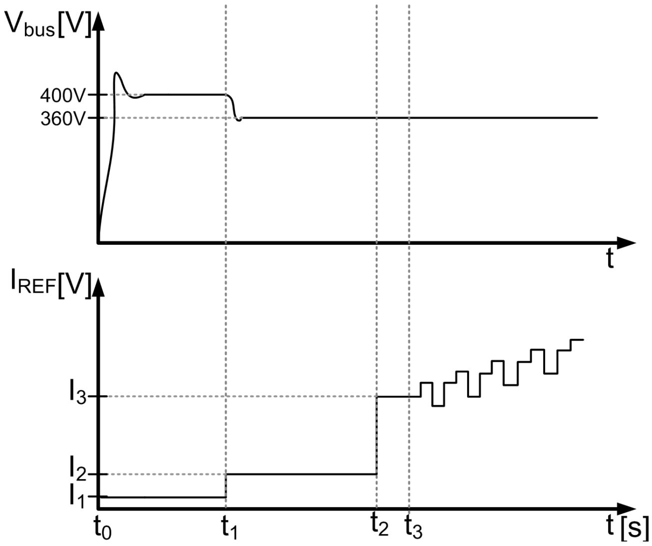

Fig. 8. Start-up sequence of the system.

At time t_0 the inverter makes its initialisations and is not connected to the step up converter. The voltage loop (blue) regulates the output voltage of the step up converter to a fixed voltage of 400V. The I_{REF} value now is very small.

At time t_1, switch S_1 turns on and the inverter starts to regulate its input voltage at 360V. The output voltage loop (blue) will saturate and impose a minimum power level that should be extracted from the renewable energy source. If this test is passed, the MPPT algorithm is started; otherwise the system enters the shutdown state.

At time t_2, the MPPT controller is activated by imposing a current reference through I_{MPPT}. I_{MPPT} has to be higher than I_2 (the saturation threshold of A_2 divided by R_5 and R_6). The smaller the gain of the voltage divider is, the smaller the I_{MPPT} reference can be, thus searching the MPP in a wider range of values.

At time t_3, the MPPT algorithm is initiated and starts to search the optimum operating point that can harvest more energy from the wind turbine.

The wind speed seen by the system is filtered by the inertia of the wind turbine. If a wind step takes place (from a high value to a lower one) and the MPPT algorithm does not respond fast enough to decrease the current reference, the input voltage starts to decrease. This will lead to an under voltage condition that will reset the system.

There are two possible solutions for this problem. The first one monitors the input voltage and if this voltage begins to drop the I_{MPPT} reference is decreased very fast. The second solution implements a feedback loop that controls the input voltage and receives its reference from the MPPT controller, Fig. 9.The responses of both control structures for a wind step change are presented in the simulations section.

The presented power topology has two switching converters. It would take too long to simulate the whole system together with the MPPT algorithm. A macromodel is created only for the input power stage.

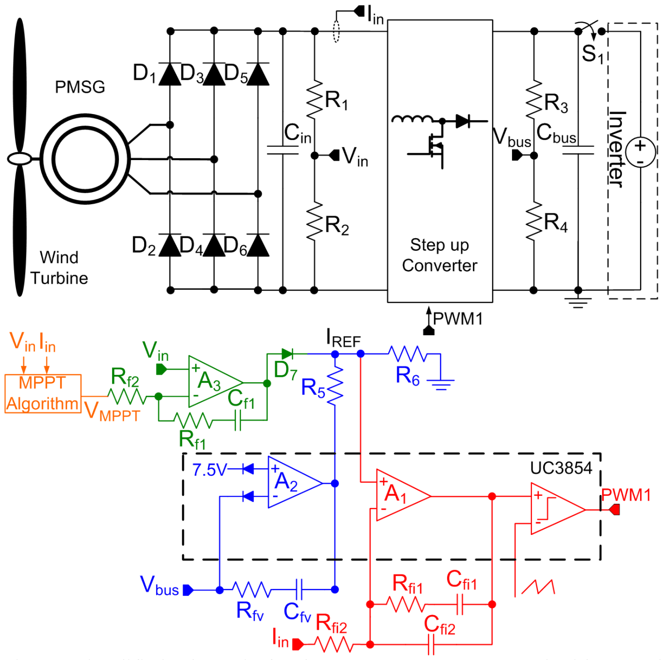

Fig. 9. Simplified schematic for the step-up converter control with control of the input voltage.

The simulation time with a macromodel can be reduced up to 40 times, thus multiple MPPT algorithm can be tested and compared in a shorter time.

The macromodel for the system presented in Fig. 9 is presented in Fig. 10. The macromodel is valid only for when the MPPT control is activated. The macromodel is only used for testing the MPPT algorithms but it can be developed to also include the functions of the step down converter by adding:

$$I_{out\_boost} = I_{in} \cdot \frac{V_{in}}{V_{bus}} \tag{7}$$

$$I_{in\_buck} = I_{out} \cdot |\sin(\omega t)|\, d_{buck}(\omega t) \tag{8}$$

IV. MPPT ALGORITHM

Before implementing the WECS, a good practice is to make a model for the wind pattern. In [14] the wind speed is described by:

$$v_{wind}(t) = v_{avg}(t) + v_{turb}(t) \tag{9}$$

where the $v_{avg}(t)$ is the low frequency component of the wind and $v_{turb}(t)$ represents the turbulences of the wind (the high

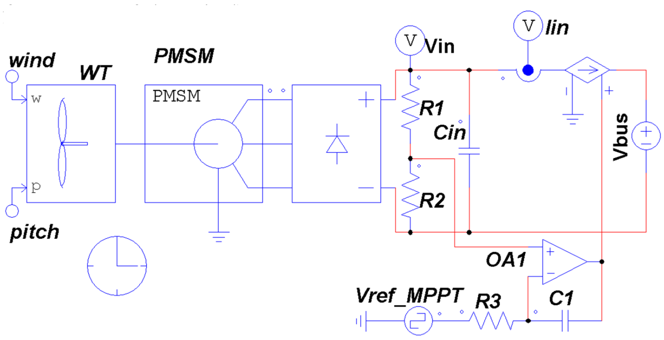

Fig. 10. Schematic of the macromodel used for the MPPT algorithm.

In the Van der Hoven spectrum can be identified the components of (9), [14]. The turbulence component is in the domain of minutes and seconds and the low frequency component varies in the domain of hours and days.

The turbulences for showing the dynamic response of the WECS are obtained by applying a Kaimal spectrum function to a white noise signal generator. The equation that describes the Kaimal normalized spectrum is:

$$\frac{n \cdot S_u(n)}{\sigma_u^2} = \frac{4 \cdot n \cdot L_{1u} / \overline{U}}{(1 + 6 \cdot n \cdot L_{1u} / \overline{U})^{5/3}} \tag{10}$$

where $\overline{U}$ is the mean wind speed, L_{1u} is the length scale. The length scale is influenced by the height above the ground and the surface roughness. The horizontal length is specified as:

$$L_{1u} = \begin{cases} 5z, z < 30m \\ 150m, z \geq 30m \end{cases} \tag{11}$$

The wind model is created in order to test the response of the MPPT algorithm. Two maximum power point tracking algorithms will be compared and the best solution will be chosen to be applied on the analysed WECS. The algorithms are: power signal feedback and P&O with three points weighting.

The algorithm perturbs the speed of the turbine with a small step, thus obtaining a measurable variation in the input power, ΔP (P_k-P_{k-1}). If ΔP>0, it means that the operating point has moved closer to the maximum power point (MPP) and the perturbation direction is maintained. If the opposite situation occurs, ΔP<0, then the current operation point was moved further apart from the maximum power point and the direction is changed.

The three weight perturbation method of the P&O algorithms has the advantage of tracking the optimum operating point and maintaining the good perturbation direction when the wind speed varies fast. The disadvantage is the need of perturbing three times the reference signal before taking a new decision.

The principle of the PSF algorithm is explained in Fig. 11. Suppose that the algorithm has found the maximum power point, of the characteristic with a wind speed of 8m/s (Power_8), in P_1. After a wind speed change from 8m/s to 10m/s the operating point, because of the voltage loop, changes from P_1 to P_2. Now, the algorithm detects that the current operating point has a power that is larger than the power of the stored characteristic. In this case the PSF increases the speed of the rotor until the power of the stored characteristic is the same with the measured power for the current operating point. Now the optimum operating point is in P_3. When the wind speed changes from 10m/s to 8m/s, the operating point changes to P_4. Now the algorithm detects that the power harvested by the system is lower than the power of the stored characteristic. In this case, the rotor will receive a command to decelerate until the new operating point has a power level equal to the power level of the stored characteristic.

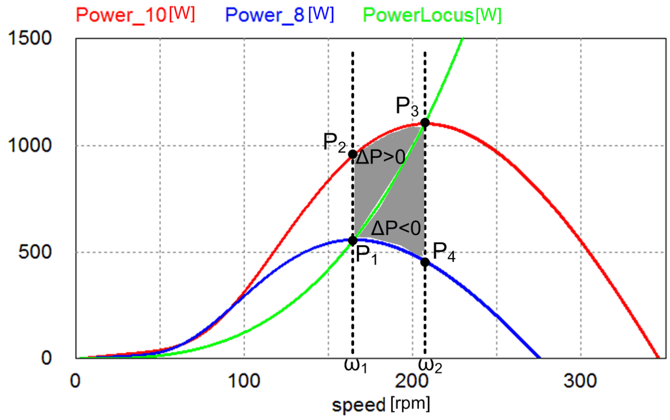

Fig. 11. PSF algorithm

The next section will present the simulations for the proposed control structure and for the MPPT algorithm with the macromodel.

V. Simulation Results

The simulation of the start-up sequence (as seen in Fig. 8) for the proposed control structure with UC3854 is presented in Fig. 12. After the MPPT controller is activated, the macromodel waveforms are also plotted. It can be seen that macromodel and the real circuit converge in the same manner at the MPP. The MPPT algorithms are tested with a wind pattern over a period of 50s.

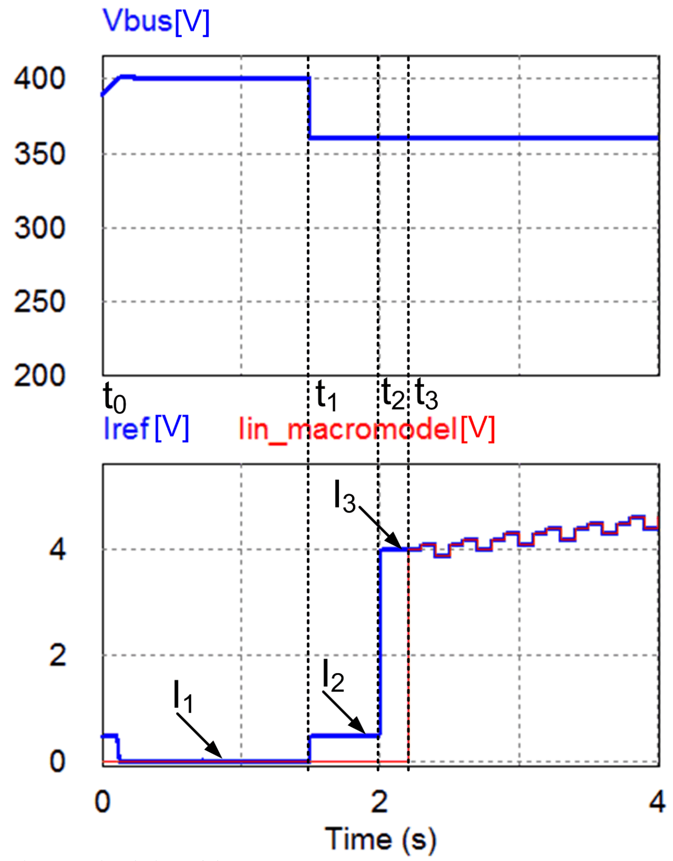

Fig. 12. Simulation of the start-up sequence.

The result of the system to a step change of the wind speed is presented in Fig. 13 for when the voltage loop is implemented (Fig. 9). For an easy explanation on how the system responds, the characteristics for two different wind speed values were considered.

It can be seen that the response of the system is analysed on the voltage-current (V-I) or on the voltage-power (V-P) characteristics. The MPP is in A and then a wind step change occurs. The voltage loop moves the operating point in B (E) and then the MPPT algorithm finds the maximum power point in C. After another wind speed change, the operating point moves to D (F) and then the MPPT algorithm finds the new optimum operating point in A.

For when only the current loop is implemented (Fig. 7), the response of the system to a wind speed change is presented in Fig. 14. The same characteristics used for the response of the voltage loop are used for the current loop.

The “ABCD” (“AECF”) hysteresis shows the response on the V-I (V-P) characteristic. In order for the system to converge when only the current loop is implemented, the MPPT algorithm must decrease its reference when the wind changes from a higher value a lower one. This can be observed on the “CD” (“CE”) segment.

The hysteresis enclosed by the system with a voltage loop is smaller than the hysteresis enclosed by the system using just a current loop. This means that the voltage loop helps the MPPT algorithm to reach faster for the optimum operating point. The next simulations will use the voltage loop configuration.

The first MPPT algorithm that is tested is the P&O algorithm with three points weighting. The simulation results are presented in Fig. 15. The total available power at the input of the turbine (Optimum) is plotted together with the harvested power (P_{in}). It can be seen that the algorithm tracks the optimum power with very little differences.

The second MPPT algorithm that is tested is the PSF algorithm. The results are illustrated in Fig. 15. It can be seen that the input voltage waveform for this algorithm is different from the input voltage waveform of the P&O algorithm. This algorithm can harvest more power than the P&O algorithm only if the stored power-speed characteristic is very accurate. If the temperature modifies, the air density constant changes then the stored characteristic changes.

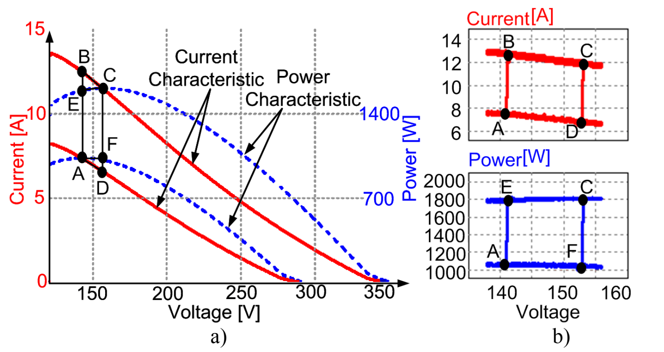

Fig. 13. System response to a wind speed change: a) with a voltage loop, b) simulation.

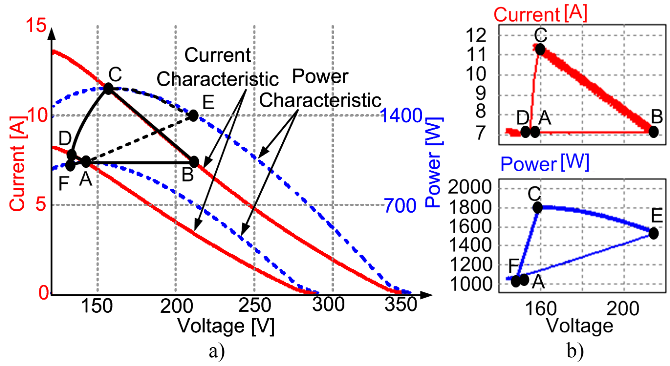

Fig. 14. System response to a wind speed change: a) with just a current loop, b) simulation

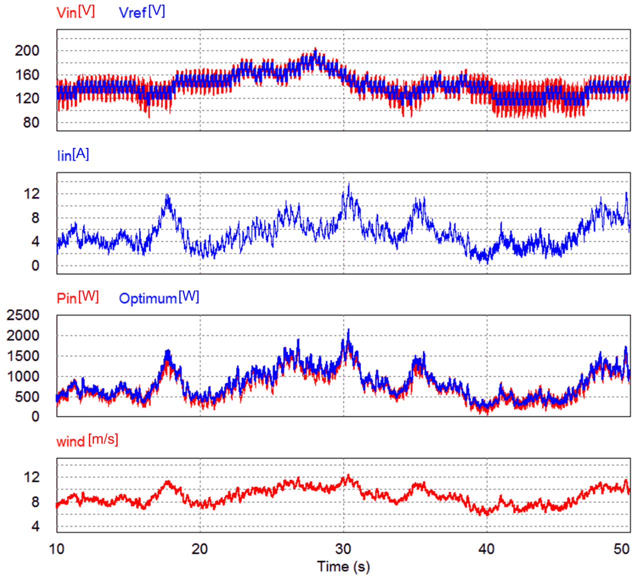

Fig. 15. Simulations with the P&O MPPT algorithm.

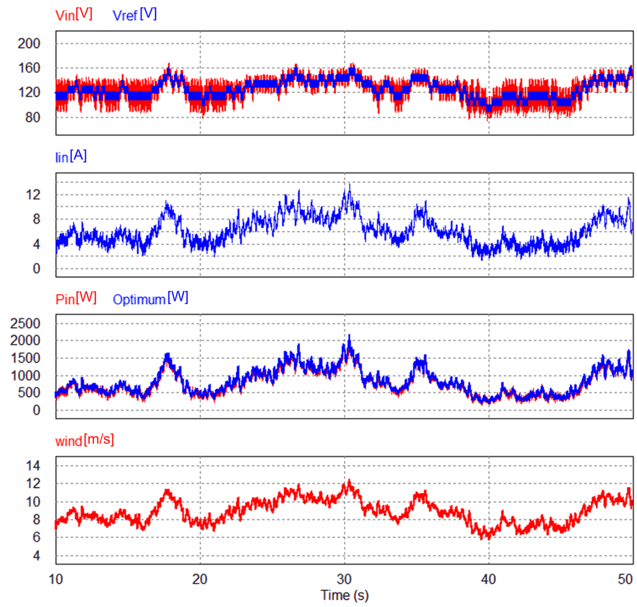

Fig. 16. Simulations with the PSF MPPT algorithm.

The input voltage has a ripple at six times the frequency of the electrical generator. Before processing the input voltage for the MPPT, this value must be filtered. If it is not filtered enough the system will only get close to the MPP and not reach it. If the input voltage is very well filtered, the system can not detect when a wind step change occurs from a high value to a lower one and a fault will occur. This is the reason that the system with voltage loop was used to test the MPPT algorithms.

The best solution for a WECS used in a small local microgrid is to use the proposed control strategy from Fig. 9 because there is no inter-dependency between the two power stages and assures a proper start-up condition for the inverter. The best solution is to use the P&O because this algorithm is system independent.

VI. Experimental Results

Partial experimental results are provided for this paper. The inverter was first tested by connecting a high DC bus and then controlled to work in a standalone configuration with a pure resistive load.

The response of the system to a current step load is presented in Fig. 17. The sinusoidal output voltage remains constant while the output current changes. Before connecting the system to the grid the response of the PLL was tested with a change in frequency, Fig. 18. The results for the inverter connected to the grid are presented in Fig. 19.

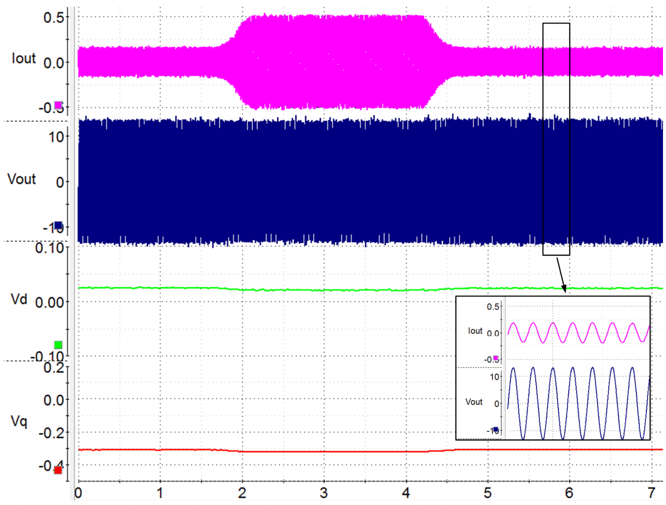

Fig. 17. Experimental results for a current step load.

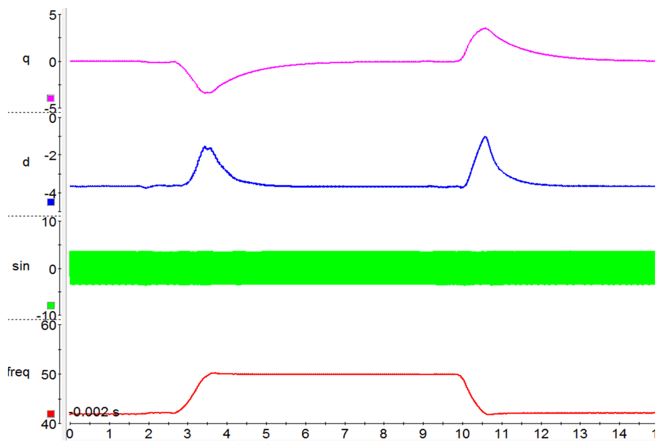

Fig. 18. Experimental results for a step change in frequency.

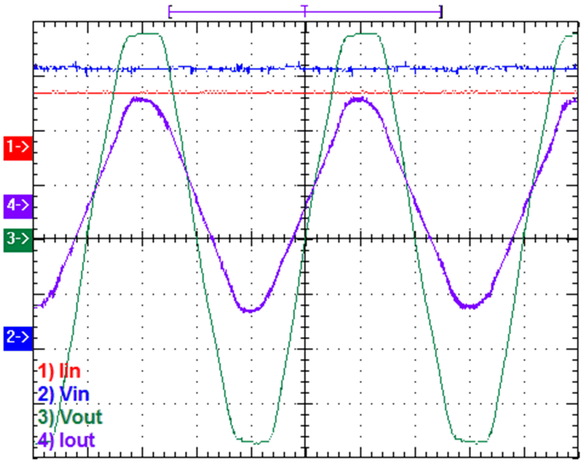

Fig. 19. Experimental results for grid connected inverter.

The distortion of the grid current is because the inverter is operated only at 10% of its total output power.

VII. CONCLUSIONS

In this paper was shown the importance of the power topology of the inverter and the overall control strategy of a wind energy conversion system. The highest performances for a WECS are obtained when two power stages are used. The efficiency of the system is high because of the power topologies. The cost of the system is low because of the modular design (the same converter is used in multiple applications) approach. The implementation of a macromodel simplifies and shortens the simulation of MPPT algorithms.

Between the two simulated maximum power point tracking algorithms, the P&O offers the greatest flexibility and is best suited for a low cost WECS.

A novel control topology was proposed that can be used in power converters. The novelty of this control structure is that allows a modular system design. The same converter can be used in multiple applications: MPPT controller for WECS, MPPT controller for photovoltaic systems, PFC, etc. The advantages of using it are: implementation with analog controller, automatic switching between the two voltage loops (input voltage control and bus voltage control), proper start-up of the inverter and current short circuit protection. Also this configuration allows easy interconnection with other systems.

The theoretical background is validated through simulation and experimental results.

For future research the proposed topology will be implemented and tested together with the inverter. The system will be connected to a small scale wind turbine. The MPPT algorithm will be implemented on a processor for a final product.

ACKNOWLEDGMENT

This work was supported by the project INNOWECS CNCS – UEFISCDI, project no. PN-II-PT-PCCA-2011-3.2-1696.

REFERENCES

[1] A.A. Aboushady, K.H. Ahmed and B.W. Williams, "Compact multi-modular design of high power DC/DC resonant converters for offshore wind energy HVDC transmission," *IECON'13,* pp. 5234-5239, Vienna, Austria, 10-14 November 2013.

[2] I. Serban and C. Marinescu, "A sensorless control method for variable-speed small wind turbines," Renewable Energy, vol. 43, pp. 256-266, 2012.

[3] W. Malan, D.J. Thrimawithana and U.K. Madawala, "Performance study on a low cost converter for micro-wind generarion systems," *IECON'13,* pp. 7191-7196, Vienna, Austria, 10-14 November 2013.

[4] D. Petreus, S. Daraban, I. Ciocan, T. Patarau, C. Morel and M. Machmoum, "Low cost single stage micro-inverter with MPPT for grid connected applications," *Solar Energy*, vol. 92, pp. 241-255, 2013.

[5] C. Nayar, H. Dehbonei and L. Chang, "An IGBT Inverter for Interfacing Small Scale Wind Generators to Single Phase Distributed Power Generation System," Australian & New Zealand Solar Energy Society, Perth, Autralia, 30th November, 2004

[6] R. Esmaili and L. Xu, "Sensorless control of permaneng magnet generator in wind turbine application," *41st Industry Applications Conference,* vol. 4, pp. 2070-2075, Tampa, USA, 8-12 Oct. 2006

[7] K. Damodarareddy, P. Nagarajaram, Md. Asif and B. Ramu, "Back-to-Back PWM converter fed PMSG wind turbine system, " *IOSR Journal of Engineering.* vol. 3(7), pp. **19**-25, 2013

[8] A. Rajaei, M. Mohamadian and A. Yazdian Varjani, "Vienna-Rectifier-based direct torque control of PMSG for wind energy application," *IEEE Transactions on Industrial Electronics*, vol. 60(7), pp. 2919 – 2929, 2013

[9] C.N. El-Khoury, H.Y. Kanaan, I. Mougharbel and K. Al-Haddad, "A review of matrix converters applied to PMSG based wind energy conversion systems," *IECON'13*, pp. 7776-7781, Vienna, Austria, 10-14 November 2013.

[10] S.A. Verne and M.I. Valla, "Direct connection of WECS system to the MV grid with multilevel converters," *Renewable Energy*, vol. 41, pp. 336-344, 2012

[11] W. Phipps, M. Harrison, & R. Duke, "New generation power converter", Australian Journal of Electrical and Electronic Engineering, Vol. 3, No.2, pp. 1-7, 2007

[12] R. Kot, M. Rolak and M. Malinowski, "Comparison of maximum peak power tracking algorithms for a small wind turbine," *Mathematics and Computers in Simulation*, vol. 91, pp. 29-40, 2013.

[13] I. Kortabarria, J. Andreu, I.M. de Alegria, J. Jimenez and J. Ignacio, "A novel adaptative maximum power point tracking algorithm for small wind turbines," Renewable Energy, vol. 63, pp. 785-796, 2014

[14] P.Gavriluta, S. Spataru, I. Mosincat, C. Citro, I. Candela and P. Rodriguez, "Complete methodology on generating realistic wind speed profiles based on measurements," ICREPQ, Santiago de Compostela, Spain, 28th-30th March, 2012

[15] C.N.M. Ho, H. Breuninger, S. Pettersson, G. Escobar and F. Canales, "A Comparative Performance Study of an Interleaved Boost Converter Using Commercial Si and SiC Diodes for PV Applications, " *IEEE Transactions on Power Electronics*, vol. 28(1), pp. 289-299, 2013.

[16] Steca Elektronik GmbH – "Steca PV grid Connected" http://www.steca.com/index.php?4ede1df6a5e9f